Earth and Planetary Science Letters 301 (2011) 493–501

Contents lists available at ScienceDirect

Earth and Planetary Science Letters

journal homepage: www.elsevier.com/locate/epsl

Thermal history and origin of the Tanzanian Craton from Pb isotope thermochronology of feldspars from lower crustal xenoliths

Jeremy J. Bellucci *, William F. McDonough, Roberta L. Rudnick

Department of Geology, University of Maryland, College Park, MD, 20742, USA

ARTICLE INFO

Article history:
Received 16 August 2010
Received in revised form 16 November 2010
Accepted 18 November 2010
Available online 16 December 2010

Editor: R.W. Carlson

Keywords:
Tanzanian Craton
thermochronology
lower crust
feldspar
anti-perthite
LA–MC-ICP-MS

ABSTRACT

Common and radiogenic Pb isotopic compositions of plagioclase and anti-perthitic feldspars from granulite-facies lower crustal xenoliths from the Labait Volcano on the eastern margin of the Tanzanian Craton have been measured via laser ablation MC-ICP-MS. Common Pb in plagioclase and a single stage Pb evolution model indicate that the lower crust of the Tanzanian Craton was extracted from mantle having a $^{238}U/^{204}Pb$ of 8.1 ± 0.3 and a $^{232}Th/^{238}U$ of 4.3 ± 0.1 at 2.71 ± 0.09 Ga (all uncertainties are 2σ). Since 2.4 Ga, some orthoclase domains within anti-perthites have evolved with a maximum $^{238}U/^{204}Pb$ of 6 and $^{232}Th/^{238}U$ of 4.3. The spread in Pb isotopic composition in the anti-perthitic feldspars yields single crystal Pb–Pb isochrons of ~2.4 Ga, within uncertainty of U–Pb zircon ages from the same sample suite. The Pb isotopic heterogeneities imply that these granulites resided at temperatures <600 °C in the lower crust of the Tanzanian Craton from ca. 2.4 Ga to the present. In concert with the chemistry of surface samples, mantle xenoliths, and lower crustal xenoliths, our data imply that the cratonic lithosphere in Tanzania formed ca. ~2.7 Ga, in a convergent margin setting, and has remained undisturbed since 2.7 Ga.

1. Introduction

Insights into the origin of the lithosphere and its thermal history can be gained through the study of deep-seated xenoliths carried in basalts and kimberlites (e.g., Carlson et al., 2005; Rudnick, 1992; Rudnick et al., 1998; Schmitz and Bowring, 2003; and references therein). In particular, Pb isotope studies of lower crustal xenoliths can provide insights into the age, composition, cooling history and origin of the lower crust (e.g., Bolhar et al., 2007; Rudnick and Goldstein, 1990; Schmitz and Bowring, 2003).

The oldest pieces of the Earth's crust, and therefore, any evidence for early Earth processes, are located in stable lithospheric blocks defined as cratons. Cratons formed in the Archean and have persisted through geologic time. Despite numerous geochemical and geophysical studies, however, debate continues regarding the origin of cratonic lithosphere and the reasons for its longevity. A defining characteristic of cratons is low surface heat flow (~40 mW/m^2) compared to crust that has been tectonically active since the Archean (>50 mW/m^2) (Nyblade and Pollack, 1993). Cratonic geotherms can be modeled as functions of surface heat flow, conductive heating from the mantle and the distribution of heat producing elements (K, Th, and U) through the lithosphere (e.g., Chapman and Pollack, 1977; Rudnick et al., 1998). A more direct approach to defining cratonic geotherms is through the application of experimentally calibrated geothermometers and geobarometers to the minerals of mantle xenoliths (e.g., Boyd, 1973; Rudnick and Nyblade, 1999). However, this approach fails to capture the time-dependent cooling of cratons and relies upon the assumption that the conditions recorded in the xenoliths reflect equilibration to present-day conditions (e.g., Michuat et al., 2007; Rudnick et al., 1998).

Temporal constraints on the formation of cratonic geotherms, which correspond to lower crustal temperatures of 400–500 °C (Chapman and Pollack, 1977; Rudnick et al., 1998), can be determined through the use of radiogenic isotopic systems with different closure temperatures applied to minerals from lower crustal xenoliths (Schmitz and Bowring, 2003). For example, U–Pb thermochronology of accessory phases (e.g., apatite, monazite, zircon, rutile) from lower crustal xenoliths of the Kaapvaal Craton indicate a slow cooling rate of 1 °C/Ma for the lower crust of that craton followed by thermal perturbations in the Proterozoic and Mesozoic (Schmitz and Bowring, 2003).

In addition to insights into thermal history, the Pb isotopic composition of xenoliths can be used to determine the time-integrated U/Pb and Th/Pb composition of the lower crust. If the common Pb isotopic composition of a rock lies on a geochron with identical age as the sample suite, then the Pb isotopic composition and, therefore, the $^{238}U/^{204}Pb$, $^{232}Th/^{204}Pb$, and $^{238}U/^{232}Th$ of the mantle source from which the crust derives may also be inferred (e.g., Bolhar et al., 2007; Möller et al., 1998; Rudnick and Goldstein, 1990).

* Corresponding author.
E-mail address: jeremy.bellucci@gmail.com (J.J. Bellucci).

0012-821X/$ – see front matter © 2010 Elsevier B.V. All rights reserved.
doi:10.1016/j.epsl.2010.11.031

2. Pb isotope systematics of feldspars

The Pb isotopic composition of a rock or mineral is composed of two components: common Pb (initial Pb inherited from the source rock) and radiogenic Pb (Pb*: Pb that is produced in the rock or mineral due to *in situ* radioactive decay of U and Th). Common Pb dominates in minerals having low $^{238}U/^{204}Pb$ and $^{232}Th/^{204}Pb$ and, thus, these minerals may record the Pb isotopic composition at the time of a rock's last equilibration, assuming the mineral has subsequently remained closed to Pb diffusion (e.g., Oversby, 1975; Zartman and Wasserburg, 1969). Common Pb can, therefore, be used to determine provenance (e.g., comparison of thorogenic Pb and uranogenic Pb in common Pb minerals can be used to distinguish different crustal domains, e.g., Möller et al., 1998), estimate the age of the rock's last isotopic equilibration, and model the $^{238}U/^{204}Pb$, $^{232}Th/^{204}Pb$, and $^{232}Th/^{238}U$ of the previous reservoir in which the Pb resided (e.g., Holmes, 1946; Houtermans, 1946; Stacey and Kramers, 1975).

If the rock in which the common Pb minerals are present is a mantle derivative, then common Pb should reflect the $^{238}U/^{204}Pb$, $^{232}Th/^{204}Pb$, and $^{232}Th/^{238}U$ of the mantle from which the rocks were derived, so long as there is no evidence for crustal contamination, mixing, or re-equilibration between minerals after initial cooling (e.g., Bolhar et al., 2007; Kamber et al., 2003; Möller et al., 1998). Oceanic basalts derive from the mantle but, due to recycling of oceanic crust at subduction zones, do not record mantle composition before ~180 Ma. In contrast, many continental basalts are contaminated by continental lithosphere (e.g., Farmer, 2003, and references therein) and may not be faithful recorders of the composition of the sublithospheric mantle, particularly for Pb, which is typically in low abundance in basalts (Farmer, 2003). Determining the $^{238}U/^{204}Pb$, $^{232}Th/^{204}Pb$, and $^{232}Th/^{238}U$ ratios in older mantle derivatives is important for tracking the changes in the mantle that have occurred through time, such as the apparent decrease in the Th/U from ~4 to ~2 from the Archean mantle to the modern mantle (e.g., Zartman and Haines, 1988; Zartman and Richardson, 2005, and references therein). For this reason, studies of underplated basalts (which are common in granulite-facies xenolith suites, e.g., Rudnick, 1992) may provide important information about the mantle composition through time.

Radiogenic Pb, which occurs in minerals with moderate to large $^{238}U/^{204}Pb$ and $^{232}Th/^{204}Pb$, can be used to constrain ages, either through U–Pb concordia (for minerals having little common Pb such as monazite, titanite, zircon, apatite and rutile), or, if there is a spread in the Pb isotopic composition, a Pb–Pb isochron. Traditionally, feldspars (both plagioclase and alkali feldspar) have been used to define the initial Pb isotopic composition of a rock (e.g., Frei et al., 1997; Ludwig and Silver, 1977; Oversby, 1978; Zartman and Wasserburg, 1969). However, some alkali feldspars contain appreciable U and, in these feldspars, Pb produced by radiogenic in-growth can be a significant component of the Pb isotopic composition, complicating its use as a strictly common Pb mineral (e.g., Housh and Bowring, 1991).

The Pb isotopic composition of a feldspar can be a mixture of several reservoirs with varying $^{238}U/^{204}Pb$. These reservoirs include common Pb, U-bearing micro-inclusions, and U-bearing exsolution lamellae (Frei and Kamber, 1995; Frei et al., 1997; Housh and Bowring, 1991). The U concentration of feldspars is correlated with the presence of an alkali component (Smith and Brown, 1988). Therefore, alkali or exsolved feldspars generally contain at least two of the aforementioned domains: a low $^{238}U/^{204}Pb$ region retaining common Pb and a higher $^{238}U/^{204}Pb$ region with more radiogenic Pb. Traditionally, step-wise leaching is used to gain access to the various Pb reservoirs in feldspars, as well as other silicate minerals, in order to construct accurate Pb–Pb isochrons (Frei and Kamber, 1995; Frei et al., 1997; Housh and Bowring, 1991).

The closure temperature (T_c) for Pb diffusion in both orthoclase and andesine (the main feldspar compositions in this study) is calculated to be ~600 °C using the methods of Dodson (1973), Pb diffusion coefficients from Cherniak (1995), assuming a spherical geometry, a grain radius of 1 mm and a cooling rate of 1 °C/Ma (similar to the lower crust of the Kaapvaal Craton of Schmitz and Bowring (2003)). If distinct Pb isotopic domains reside in a single feldspar crystal, the temperature must have been below 600 °C. Furthermore, these different domains should produce a Pb–Pb or U–Pb isochron that yields the time at which the feldspars cooled below the closure temperature.

Here we show that *in situ* Pb isotopic measurements of feldspars by laser ablation multi-collector inductively coupled plasma–mass spectrometry (LA–MC-ICP-MS) provides the spatial resolution in individual heterogeneous feldspars that is needed to construct Pb–Pb isochrons. We apply this method to lower crustal xenoliths carried in recent alkali basalts erupted on the margin of the Tanzanian Craton in order to elucidate the thermal history of cratonic lower crust and characterize the Pb isotopic composition of its mantle source.

3. Geologic setting

The Tanzanian Craton comprises Archean terrains that amalgamated ca. 2.6 Ga (Maboko, 2000; Manya et al., 2006) (Fig. 1). The exposed surface of the Tanzanian Craton is comprised of tonalites, trondhjemite, and granodiorites (TTGs), gneisses, and greenstone belts (Schulter, 1997), all of which have Archean Nd model ages and U–Pb zircon ages of ~3.0 Ga and 2.6 Ga, respectively (Maboko, 2000; Manya et al., 2006; Möller et al., 1998). Both geophysical and xenolith evidence indicate that the Tanzanian Craton has a stable, deep lithospheric keel (Chesley et al., 1999; Lee and Rudnick, 1999; Ritsema et al., 1998). The lithosphere of the Tanzanian Craton is characterized by low surface heat flow (34 ± 4 mW/m^2) (Nyblade et al., 1990) and high seismic velocities in the mantle to a depth of 150 ± 20 km (Weerarante et al., 2003).

To the east of the Tanzanian Craton lies the western granulite section of the Mozambique Belt (Fig. 1) and to the southeast lies the

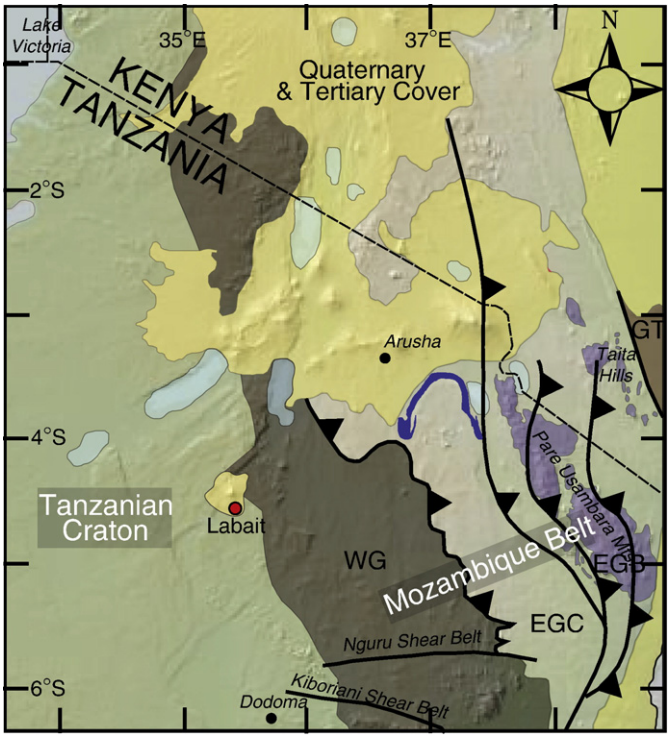

Fig. 1. Simplified geologic map of northern Tanzania (modified after Cutten et al., 2006; Fritz et al., 2009). W.G.: Western granulites; E.G.C.: Eastern granulite cover, E.G.B.: Eastern granulite basement; G.T.: Galena Terrane. Map created by M. Blondes.

Usagaran Belt. The Mozambique Belt formed in a Himalayan-scale orogeny (Fritz et al., 2009) and marks the suture between east and west Gondwana (Cutten et al., 2006; Fritz et al., 2009). The western granulites have Archean Nd model ages (Möller et al., 1998) and U–Pb zircon ages of 2.6–2.8 Ga (Johnson et al., 2003) and were metamorphosed to granulite facies in the Archean, 50–100 Ma after their emplacement into a continental arc (Johnson et al., 2003). Subsequently, the western granulites were then reworked during the Pan-African Orogeny ca. 560 Ma (Blondes et al., 2009; Cutten et al., 2006). The southeastern Tanzanian Craton was the overriding plate of a subduction zone ca. 2.0 Ga resulting in the Usagaran mountain belt and suture (e.g., Collins et al., 2004; Möller et al., 1995). There is no evidence for a 2.0 Ga event in northern Tanzania (Blondes et al., 2009; Cutten et al., 2006; Fritz et al., 2009; Johnson et al., 2003; Mansur, 2008).

The East-African Rift (EAR) surrounds the Tanzanian Craton, forming the eastern (Gregory) and western (Lake Albert) branches, which first developed at ca. 30–50 Ma, with volcanism continuing today (Dawson, 1992; Nyblade and Brazier, 2002). The Labait Volcano lies on the eastern edge of the Tanzanian Craton (4°34′13.76″S, 35°26′1.60″E), where the rift splays into a wide region of extension and volcanism. Labait erupted tuff and olivine melilitite carrying a wide array of mantle and crustal xenoliths at ~400 Ka (Dawson et al., 1997; Rudnick et al., 1999). Mantle peridotite xenoliths from Labait yield pressure–temperature (P–T) estimates that scatter about a 50 mW/m^2 geotherm and indicate derivation depths of 50–150 km (Lee and Rudnick, 1999). Rhenium depletion Os isotope model ages for the mantle xenoliths range up to 2.8 Ga (Burton et al., 2000; Chesley et al., 1999). Some mantle peridotites from the Labait volcano have experienced overprinting and heating by rift magmas (Aulbach et al., 2008; Chesley et al., 1999; Lee and Rudnick, 1999; Rudnick et al., 1999), but the extent to which the rift has affected the lower crust of the Tanzanian Craton is unknown.

4. Samples

Petrographic, mineral chemistry, whole rock major and trace element geochemistry, Rb–Sr and Sm–Nd isotopic data, as well as some U–Pb zircon ages for the Labait granulite xenoliths are presented in Mansur (2008). U–Pb analyses of zircon and accessory phases from these samples are presented in Blondes et al. (2009). The xenoliths for this study fall into five different groups, based on major mineralogy and trace element chemistry: two pyroxene granulites (n = 7), garnet orthopyroxene granulites (n = 2), two pyroxene hornblende granulites (n = 2), and anorthosite (n = 1), all of which derive from the lower crust (Mansur, 2008). In addition, we studied a xenolithic two-mica granite (n = 1). Plagioclase and/or anti-perthite (orthoclase exsolved from albite) from eleven granulite-facies xenoliths, spanning all varieties, were analyzed here, as well as anti-perthite from the granite xenolith. Table 1 lists the major mineralogy of these samples.

The Labait xenoliths, like most other granulite-facies lower crustal xenoliths, have mafic compositions with <54 wt.% SiO_2 (Mansur, 2008). They are enriched in light rare-earth elements (REE), have negative Ti and Nb anomalies, and have high La/Nb ratios (between 1.3 and 7.1), all of which suggest formation as a crystallized basaltic melt in an arc setting (Mansur, 2008). Additionally, these samples show striking depletions in Rb, Cs, Th and U, which has been interpreted to have occurred during granulite facies metamorphism (Mansur, 2008). Based on two-pyroxene Fe–Mg exchange thermobarometry, the Labait xenoliths record a broad range of equilibration temperatures from 480° to 850 °C, with most <670 °C (assuming a pressure of equilibration of 1 GPa or 33 km depth) (Mansur, 2008). The equilibration conditions for these xenoliths are similar to those of the felsic granulites found in the western granulite belt (Johnson et al., 2003). One sample, LB04-87, is a granite, which is distinct in both mineralogy and texture (Table 1), and likely derived from the shallow crust. Importantly, no radiogenic Pb is observed in mineral separates of apatite (closure temperature ~450 °C for 100 μm crystals cooled at 2 °C/Ma, Cherniak et al., 1991) from the granulite-facies xenoliths, demonstrating their derivation from the present-day lower crust, where the temperature must have exceeded 450 °C (Blondes et al., 2009). U–Pb zircon ages and Nd model ages for these samples, 2.643 ± 0.002 Ga and 2.9–3.8 Ga, respectively (Blondes et al., 2009; Mansur, 2008), mark their formation during the Archean. These ages coincide with the timing of greenstone belt volcanism in the northern part of the Tanzanian Craton (Manya et al., 2006) and overlap the 3.0–3.1 Ga Nd model ages from surface samples from the Tanzanian Craton (Möller et al., 1998).

Table 1
Samples and major mineralogy.

Sample #	Rock type	Major mineralogy
LB04-09	2 Px gran	Plagioclase orthopyroxene, clinopyroxene
LB04-19	2 Px gran	Anti-perthite, orthopyroxene, clinopyroxene
LB04-38	2 Px gran	Plagioclase, orthopyroxene, clinopyroxene
LB04-43	2 Px gran	Plagioclase, orthopyroxene, clinopyroxene
LB04-50	2 Px gran	Anti-perthite, orthopyroxene, garnet
LB04-65	2 Px gran	Anti-perthite, orthopyroxene, clinopyroxene
LB04-87	Granite	Anti-perthite, orthoclase, quartz, biotite, muscovite
LB04-48	2 Px Hbl gran	Plagioclase, clinopyroxene, orthopyroxene, hornblende
LB04-27	Anorthosite	Plagioclase, garnet, orthopyroxene
LB04-39	Gt Opx gran	Plagioclase, orthopyroxene, garnet
LB04-91	Gt Opx gran	Anti-perthite, orthopyroxene, garnet

Gran: Granulite, Px: Pyroxene, Gt: Garnet, Hbl: Hornblende, Bt: Biotite, Opx: Orthopyroxene.

Feldspars from the Labait xenoliths consist of both plagioclase and anti-perthite. The plagioclase composition is $An_{32-55}Ab_{47-64}Or_{0-6}$, while the orthoclase, in anti-perthite, has a composition of $An_{1-3}Ab_{7-23}Or_{73-91}$ (Mansur, 2008). One sample, LB04-27, is an anorthosite having plagioclase with a bytownite composition ($An_{87-89}Ab_{11-12}$) (Mansur, 2008). All orthoclase observed in these samples are part of the anti-perthite, and therefore, any analyses performed on orthoclase were performed in the same time-resolved analyses as the plagioclase.

5. Analytical methods

5.1. Pb isotopic measurements

Samples were prepared either as polished rock slabs mounted in epoxy or 50–60 μm polished thick sections. The Pb isotopic compositions were determined *in situ* via LA–MC-ICP-MS using a frequency-quintupled solid-state Nd:YAG laser system (213 nm wavelength) and a Nu Plasma MC-ICP-MS (following Kent, 2008a,b; Paul et al., 2005). Full analytical details are provided in the Supplementary materials and a brief overview is given below.

Ion beams of ^{200}Hg, ^{202}Hg, and ^{204}Pb/Hg were monitored using parallel ion counters, whereas isotopes ^{201}Hg, ^{206}Pb, ^{207}Pb, and ^{208}Pb were detected simultaneously as ion currents in parallel Faraday cups equipped with 10^{11} Ω resistors. In order to correct for the isobaric interference of ^{204}Hg on ^{204}Pb, ^{200}Hg/^{202}Hg was monitored to allow subtraction of a fractionation-corrected abundance of ^{204}Hg. The Hg fractionation factor was calculated using the exponential law and assuming natural isotopic abundances (de Laeter et al., 2003). The Hg fractionation factor was then applied to the ^{204}Hg/^{202}Hg ratio and subsequently the ^{204}Hg signal was stripped from the ^{204}Pb signal. The contribution of ^{204}Hg on the ^{204}Pb signal was typically <0.7%. Backgrounds were measured on-peak for 60 s prior to ablation with the laser on and shuttered. The average of each signal's background was subtracted in real time from each individual measurement collected at intervals of 0.2 s using the Nu Plasma time resolved software. For accurate isotopic measurements, two corrections must be applied to the background-corrected data: 1) mass fractionation corrections and 2) ion counter-Faraday cup gain corrections. Mass

fractionation effects are corrected using standard sample bracketing using SRM NIST 612 as the reference standard and calculating the fractionation factor of $^{208}Pb/^{206}Pb$ using the exponential fractionation law. Using the fractionation factor from $^{208}Pb/^{206}Pb$, an expected $^{20x}Pb/^{204}Pb$ (x = 8, 7, or 6) can be calculated. Discrepancies between the Faraday cup and ion counter gains can be corrected by using the ratio between the measured and calculated $^{20x}Pb/^{204}Pb$ values of SRM 612 (Baker et al., 2004).

While the analytical precision using this method is largely dependent on the Pb concentration in the sample, which can range between 10 and 20 μg/g, repeat measurements (n = 85) over a several month period of the basaltic glass standard BCR 2-g, which contains ~10 μg/g Pb, yielded accuracies of ≤±0.1% for $^{20x}Pb/^{204}Pb$ and an external reproducibility of ≤±0.5% (2σ) for $^{20x}Pb/^{204}Pb$. A detailed discussion of the accuracy and precision of this method is given in the Supplementary materials.

5.2. U–Pb

The U–Pb ratio in a feldspar from one sample (gt-opx granulite LB04-91) was measured by LA–ICP-MS utilizing the same laser ablation system described above coupled to a ThermoFinnigan Element 2 ICP-MS. Ten spots, 40 μm in diameter, were analyzed along a Pb-isotope laser ablation track (Fig. 5). Further details of the analytical conditions and results are given in the Supplementary materials.

5.3. Solution analyses

The Pb isotopic composition of the host basalt was analyzed by both solution MC-ICP-MS and LA–MC-ICP-MS. The solution measurements were performed using parallel Faraday cups. Pb was purified from dissolved rock using standard HBr anion chromatography. Mass fractionation was accounted for using the exponential fractionation law through the addition of Tl (e.g., Baker et al., 2004). The lab blank was measured to be ~330 pg, which corresponds to a sample/blank ratio of ~10^3. The results are within uncertainty (≤0.2%) of the LA–MC-ICP-MS. This uncertainty is similar to that obtained for measurements of standard materials. Data are provided in the Supplementary materials.

6. Results

The Labait host melilitite has a Pb isotopic composition similar to that of other rift basalts from Northern Tanzania (e.g., Paslick et al., 1995); see the Supplementary materials for comparison.

The Pb isotopic composition of plagioclase and anti-perthite from the Labait lower crustal xenoliths (n = 137) are presented in Figure 2 (data tables are provided in the Supplemental materials). Anti-perthites in six samples (four two-pyroxene granulites LB04-19, LB04-50, LB04-82, one gt-opx granulite, LB04-91 and the granite, LB04-87) display a significant spread in Pb isotopic compositions. Plagioclase in a further six samples (which include specimens from all four groups of granulites) show no significant spread in their Pb isotopic compositions (all analyses are within analytical uncertainty of each other) and all, except that from the anorthosite, have non-radiogenic compositions that plot near the 2.7 Ga geochron (Fig. 2). By contrast, the anorthosite plagioclase has relatively radiogenic Pb that plots near the present-day geochron. During the analysis of plagioclase from the granite, LB04-87, inclusions of very radiogenic Pb ($^{206}Pb/^{204}Pb$~28) were intersected, as reflected in the time resolved spectra. We assume that these inclusions are apatite, which is present in the backscatter electron images of LB04-87 (Fig. 3). A figure of the time resolved spectra from this analysis is located in the Supplementary materials.

Isochrons were calculated using the program Isoplot (Ludwig, 2003) for each anti-perthite grain, multiple feldspar grains (multiple feldspar) within a given sample, and for each group of samples: 2 px granulites, gt-opx granulites, hbl granulites and the granite (Table 2, Figs. 3 and 6). Figure 3 illustrates single crystal (±inclusions) isochrons for gt-opx granulite LB04-91 and granite LB04-87. The isochron for sample LB04-91 is defined by a combination of plagioclase and orthoclase zones in a single crystal of anti-perthite. The isochron for sample LB04-87 is defined by both anti-perthite and an apatite inclusion. All isochrons are Archean. The average age of the individual anti-perthites is ~2.4 Ga, while multiple phase/sample suite isochron ages average ~2.7 Ga (Table 2), which is coincident with the U–Pb zircon ages from the Labait xenoliths from Mansur (2008) and Blondes et al. (2009).

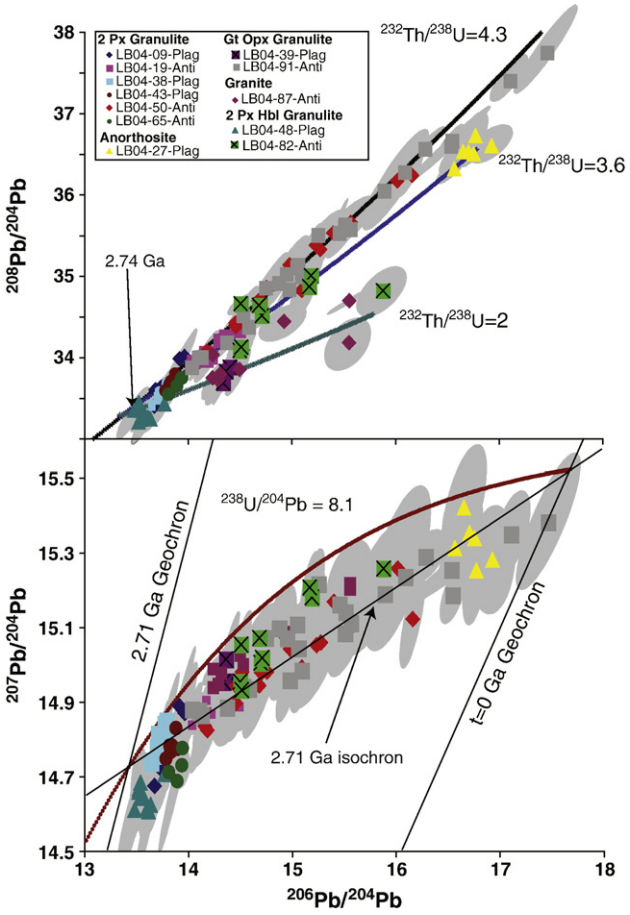

Fig. 2. Pb isotopic data for feldspars in lower crustal xenoliths from the Tanzanian Craton. The data lie along a 2.71 Ga isochron, shown for reference (calculated with Isoplot, Ludwig, 2003), which is an age that is identical to the average of all other isochrons from individual samples suites (Table 2). A single-stage Pb evolution model from primordial Pb (Chen and Wasserburg, 1983) is illustrated for a $^{238}U/^{204}Pb$ of 8.1 and $^{232}Th/^{238}U$ of 4.3. Evolution of $^{208}Pb/^{204}Pb$ and $^{206}Pb/^{204}Pb$ at $^{232}Th/^{238}U$ of 2 and 3.6 are shown as fractionation of Th from U after extraction from a crustal source having $^{232}Th/^{238}U$ of 4.3 formed at 2.71 Ga. Error ellipses represent $2\sigma_{mean}$ of each analysis.

The Pb isotopic composition of the Labait feldspars, even with radiogenic in-growth, plot to the left of the present-day geochron. The data form a linear array stretching between the present-day geochron and the 2.71 Ga geochron. The trend seen in 2 px granulite LB04-38 is a mass fractionation trend and the data points are indistinguishable within analytical uncertainty.

7. Discussion

7.1. Origin of the linear trends

Linear trends in isotopic data can either reflect mixing between two isotopically distinct components or result from the in-growth of the radiogenic daughter product. Only the latter has any age significance.

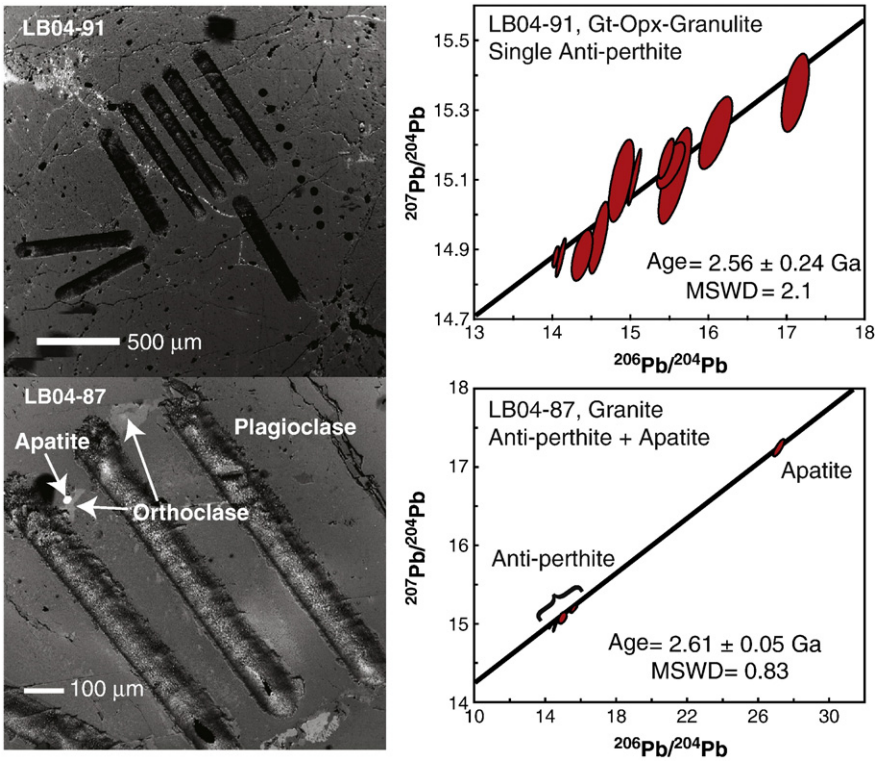

Fig. 3. Top left: Backscatter electron image of plagioclase/anti-perthite from sample LB04-91 with corresponding single crystal anti-perthite isochron, shown with laser tracks and laser ablation pits. The multiple data points (top right) are from discrete regions in the feldspar revealed in the time-resolved spectra of the ablation lines. Bottom left: Backscatter electron image of plagioclase, anti-perthite, and apatite inclusions from granite LB04-87 and corresponding isochron (bottom right). The backscatter electron images were taken using a JEOL JXA-8900 SuperProbe. Photos were taken in beam scan mode with an accelerating voltage of 15 kV.

One possible source of radiogenic Pb that may have been mixed into the xenoliths is the host lava. Figure 4 shows a mixing trajectory between the least radiogenic plagioclases (~20 µg/g Pb, from samples LB04-48 and LB04-38) and the Labait melilitite (~8 µg/g). Many of the feldspar analyses plot beyond analytical uncertainty of this mixing line, although some overlap it. To achieve this range in Pb isotopic compositions via host basalt mixing, up to ~80% of the Pb in the most radiogenic samples must have originated from the basalt. This level of mixing is untenable on two accounts. First, the whole-rock Nd isotopic compositions and trace element compositions of the samples do not record any such mixing (Mansur, 2008). Second, in order for Pb from the basalt to enter the feldspars, the samples would need to be heated above 600 °C (T_c for Pb in feldspar) during the xenolith's entrainment within the basalt. Such heating is precluded on the basis of U–Pb thermochronology of titanite (T_c>550 °C) and apatite (T_c>450 °C) from lower crustal xenoliths hosted in a similar alkali basalt from a near-by locality (Lashaine, Blondes et al., 2009). Apatite in these samples was open to Pb diffusion at the time of eruption, like those in the Labait xenoliths, but titanite records concordant Paleozoic $^{206}Pb/^{238}U$ ages, reflecting slow cooling following the Pan-African Orogeny. Collectively, these results indicate that the samples remained above apatite closure temperature but below titanite (and feldspar) closure temperature for hundreds of millions of years—more

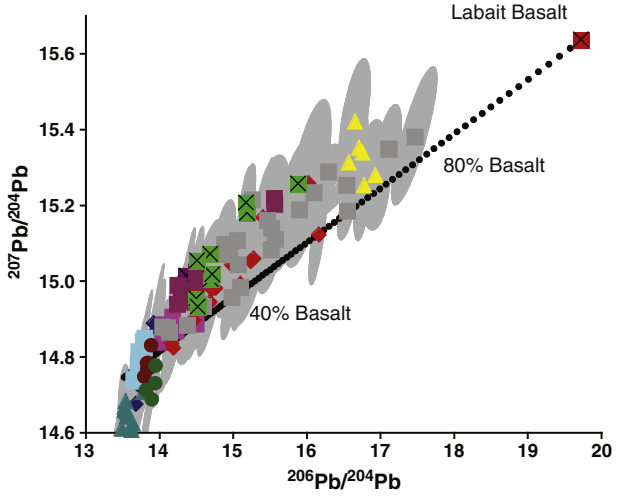

Fig. 4. Mixing diagram from least radiogenic Pb composition in the Labait lower crustal xenolith feldspars (20 µg/g) and the Labait Basalt (8 µg/g). Error ellipses are $2\sigma_{mean}$ of each feldspar analysis and the error on the Labait host lava is smaller than the symbol.

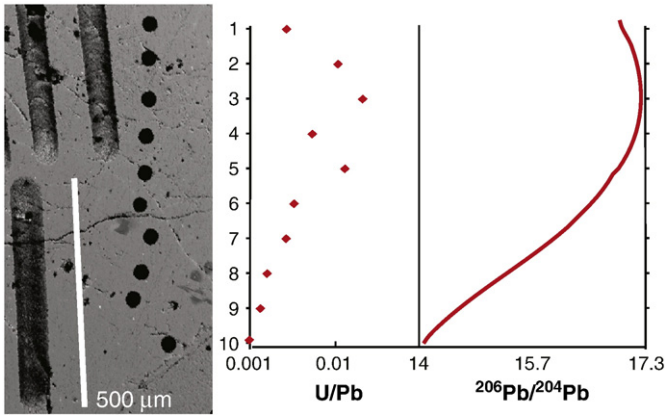

Fig. 5. Laser ablation pits from anti-perthite in LB04-91 (see Fig. 2) and corresponding U/Pb measurements performed as spot analyses with LA–ICP-MS, indicating variable U–Pb ratios on a micron scale within the anti-perthite. Right panel shows an estimate of the corresponding $^{206}Pb/^{204}Pb$, based on the time-resolved spectra, matched with the spot U analyses.

Table 2
Summary of Pb–Pb ages from Labait xenoliths.

Sample suite	Sample (s)	Minerals	Age (in Ga)	2σ
2 Px granulite	LB04-19	Multiple plagioclase	2.96	1.50
2 Px granulite	LB04-43	Multiple plagioclase	3.54	0.50
2 Px granulite	LB04-50	Single anti-perthite	2.74	0.43
2 Px granulite	LB04-50	Single anti-perthite	2.30	0.60
2 Px granulite	LB04-50	Anti-perthite, ilmenite	2.51	0.35
2 Px granulite	LB04-65	Anti-perthite, apatite	2.42	0.69
2 Px granulite	LB04-65	Anti-perthite, apatite	2.75	1.60
2 Px granulite	LB04-65	Multiple ant-perthite, multiple apatite	2.32	0.68
2 Px granulite	LB04-09, LB04-19, LB04-38, LB04-43, LB04-50, LB04-65		2.71	0.24
Gt-Opx-granulite	LB04-91	Single anti-perthite	2.56	0.24
	LB04-91	Single anti-perthite	2.15	0.68
	LB04-91	Multiple anti-perthite	2.42	0.26
Gt-Opx granulite	LB04-39, LB04-91		2.38	0.23
2 Px Hbl gran	LB04-82	Single anti-perthite	2.48	0.59
		Multiple anti-perthite, pyroxene	2.61	0.76
2 Px Hbl gran	LB04-48, LB04-82		3.40	0.25
Granite	LB04-87	Anti-perthite–apatite inclusion	2.68	0.15
	LB04-87	Anti-perthite–apatite inclusion	2.61	0.05
	LB04-87	Multiple anti-perthie, apatite	2.62	0.25
		Average age of anti-perthite	2.44	0.41
		Average of non anti-perthite ages	2.71	0.73
		Isochron of the entire sample suite	2.71	0.09

than two orders of magnitude longer than the duration of rift volcanism in northern Tanzania. Similar results were obtained for kimberlite-hosted lower crustal xenoliths from the Kaapvaal Craton (Schmitz and Bowring, 2003). We conclude that mixing with the host basalt did not generate the linear correlation seen in the plot of $^{206}Pb/^{204}Pb$ vs. $^{207}Pb/^{204}Pb$.

Because the U/Pb ratio of anti-perthite from gt-opx granulite LB04-91 shows over an order of magnitude change over a distance of ~800 μm, and correlates with the $^{206}Pb/^{204}Pb$ ratio (Fig. 5), we suggest that the linear correlation reflects an isochron, rather than mixing between two ancient Pb components. Below we explore the thermochronological implications of the feldspar isochrons.

7.2. Thermochronometry

Individual feldspars in five samples (2 px granulites LB04-19, LB04-50, LB04-82, gt-opx granulite LB04-91 and the granite, LB04-87) are heterogeneous with respect to their Pb isotopic compositions, indicating that they have resided at temperatures below ~600 °C, given the closure temperature of Pb in feldspar calculated above. The Pb isotopic heterogeneities reflect several reservoirs of radiogenic Pb, similar to other U-bearing silicate minerals (Frei and Kamber, 1995) and yield isochron ages of ~2.4 Ga. This result demonstrates that the Pb–Pb system in feldspars is a viable thermochronometer in rocks having coarse-grained (mm) feldspars, significant age, and U and Th concentrations. Because feldspars from the Labait xenoliths record a range of Pb isotopic compositions, the temperature of the lower crust of the Tanzanian Craton must not have been elevated above 600 °C at any time following 2.4 Ga, including during the Pan-African Orogeny (ca. 560 Ma) and the development of the East African Rift.

Given the spread in Pb isotopic values and the isochron age, a maximum $^{238}U/^{204}Pb$ can be calculated for the feldspar grains. The

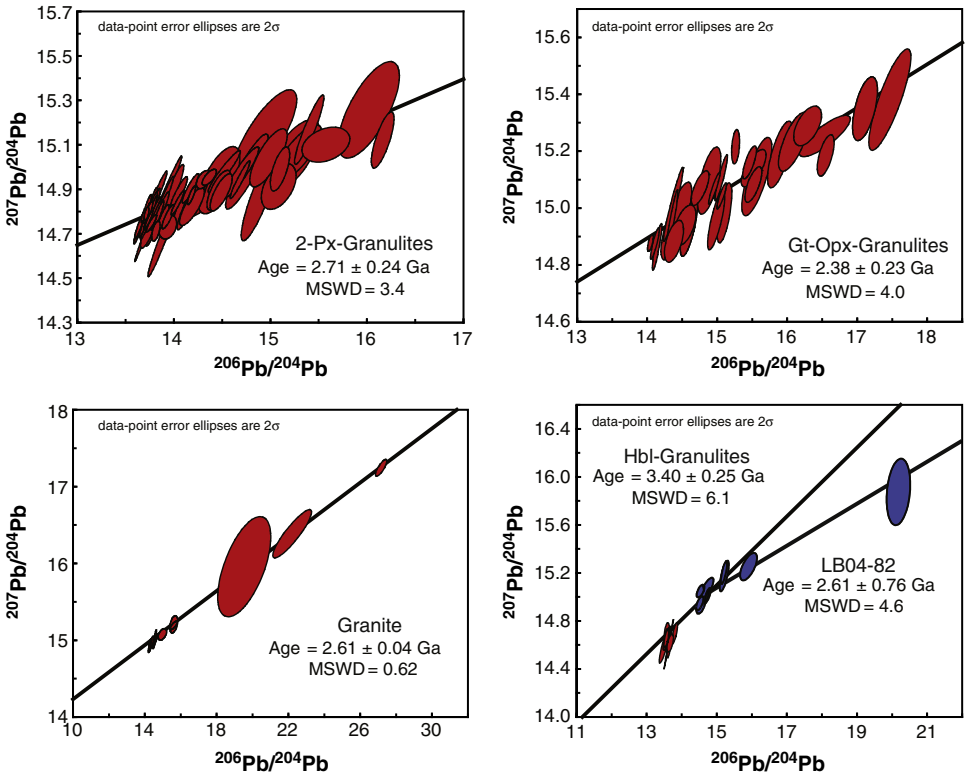

Fig. 6. Isochrons calculated for each sample suite, two pyroxene granulites, gt-opx granulites, granite, and Hbl granulites.

largest range in Pb isotopic values for a single feldspar is seen in gt-opx granulite LB04-91, which has $^{206}Pb/^{204}Pb$ varying from 14.87 to 15.38, corresponding to a maximum $^{238}U/^{204}Pb$ of 6. Most of the samples fall on a linear trend on the $^{208}Pb/^{204}Pb$ vs. $^{206}Pb/^{204}Pb$ diagram, corresponding to a $^{232}Th/^{238}U$ of 4.3. Three samples, one from each of three different lithological groups, fall off this trend: gt-opx granulite LB04-39, the single anorthosite, LB04-27 and the granite LB04-87. Assuming these samples were extracted at the same time and from the same mantle source as the other Labait xenoliths (because they follow the same trend as the other samples in the $^{207}Pb/^{204}Pb$ vs. $^{206}Pb/^{204}Pb$ plot), their Pb isotopic composition can be modeled with a $^{232}Th/^{238}U$ of 2, 3.6 and 2, respectively (Fig. 2). All of the calculated $^{232}Th/^{238}U$ ratios are within the range of the whole rock Th/U (0.7–5.6, Mansur, 2008). The variable $^{232}Th/^{238}U$ ratios in the feldspars of these three samples illustrate the potential of the $^{208}Pb/^{204}Pb$ vs. $^{206}Pb/^{204}Pb$ composition in feldspars to be a more sensitive discriminator of provenance than the $^{207}Pb/^{204}Pb$ vs. $^{206}Pb/^{204}Pb$ composition.

7.3. Pb isotopic composition of the lower crust and mantle source

In addition to providing constraints on the thermal history of the lower crust of the Tanzanian Craton, the common Pb isotopic composition of Labait feldspars can also be used to place constraints on its age and origin. Based on trace element analyses, most of the Labait lower crustal xenoliths (in particular, the two pyroxene granulites) likely crystallized as basalts from an arc setting and subsequently underwent granulite facies metamorphism (Mansur, 2008). Considering that all of these xenoliths have relatively low equilibration temperatures (Mansur, 2008), and lie on a linear array in $^{207}Pb/^{204}Pb$ vs. $^{206}Pb/^{204}Pb$ space (except hornblende granulite LB04-48), we interpret them to have formed from the same mantle reservoir at the same time. Therefore, we group all of the Pb isotopic compositions from this suite of xenoliths to get an age of lower crust extraction from the mantle of 2.71 ± 0.09 Ga (Table 2). This mantle extraction age is similar to that of the western granulites (Johnson et al., 2003). In addition, the age recorded by the anti-perthitic feldspars (~2.4 Ga) could date the age of metamorphism of the lower crust to granulite facies, which is similar to the metamorphic event seen by the western granulites, occurring 50–100 Ma after extraction from the mantle.

The Pb isotopic compositions of the all of the feldspars from the Labait lower crustal xenoliths, except those in hornblende granulite LB04-48, lie within error of a 2.71 Ga isochron (Fig. 2). The 2.71 Ga isochron intersects the 2.71 geochron (Holmes, 1946) at $^{206}Pb/^{204}Pb = 13.4 \pm 0.4$ and $^{207}Pb/^{204}Pb = 14.7 \pm 0.4$ (2σ), near the common Pb isotopic composition of feldspars in the two least-radiogenic samples, LB04-38 and LB04-48. Using a single-stage Pb evolution model, the primordial Pb isotopic composition of Canyon Diablo troilite (Chen and Wasserburg, 1983), and assuming the intersection between the Labait isochron and geochron represents the isotopic composition of the Tanzanian Craton crust at the time of its extraction from the mantle, this crust derived from a mantle source with a $^{238}U/^{204}Pb$ of 8.1 ± 0.3 (Fig. 2). Similarly, the $^{238}U/^{204}Pb$ value for the mantle source was 35 ± 1, with a $^{232}Th/^{238}U$ of 4.3 ± 0.1 (Fig. 2). This $^{238}U/^{204}Pb$ is similar to that found for Archean komatiites from Canada, Australia, and Africa that indicate mantle $^{238}U/^{204}Pb$ values at ~2.7 Ga of 7.8–8.5 (Chauvel et al., 1993 and Dupré and Arndt, 1990). The inferred $^{232}Th/^{238}U$ is consistent with previous observations that the Archean mantle had a $^{232}Th/^{238}U$ of ~4 (e.g., Zartman and Haines, 1988; Zartman and Richardson, 2005, and references therein).

Two samples do not follow the general trends defined by the rest of the suite. The anorthosite (LB04-27) has unusually radiogenic plagioclase, which lies close to the present-day geochron. The anorthosite does not fall on the mixing trend with the Labait basalt, suggesting that it may have derived from a deeper (hotter) level than the other samples and may have equilibrated with U-bearing phases more recently. In contrast, plagioclase in hornblende granulite LB04-48 has the least radiogenic Pb isotopic composition of the entire suite and lies below the linear trend defined by the other samples in both $^{208}Pb/^{204}Pb$ vs. $^{206}Pb/^{204}Pb$ and $^{207}Pb/^{204}Pb$ vs. $^{206}Pb/^{204}Pb$ plots (Fig. 2). The non-radiogenic composition of the common Pb in this sample could reflect its derivation from somewhat older material present in the cratonic lower crust.

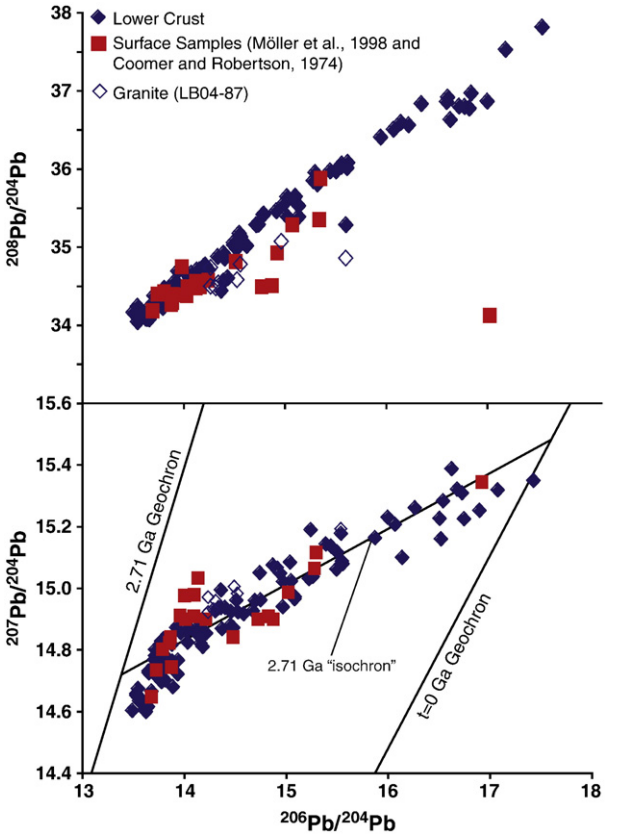

Fig. 7. Pb isotopic data for feldspars in lower crustal xenoliths compared to surface feldspars (Möller et al., 1998) and galenas/pyrites (Coomer and Robertson, 1974) from the Tanzanian Craton. The granitic sample (LB04-87) is shown in open symbols.

The common Pb isotopic composition of the Tanzanian lower crust overlaps with the Pb isotopic composition of feldspars and galenas from outcrops within the Tanzanian Craton, in a similar, slightly curved array (Fig. 7) (Coomer and Robertson, 1974; Möller et al., 1998). The similarity between Pb isotopic compositions of surface samples and lower crustal xenoliths indicates a similar provenance, and therefore, similar model ages for the upper and lower crust. The linear relationship of the Pb isotopic composition of lower crustal feldspars and surface samples in both $^{208}Pb/^{204}Pb$ vs. $^{206}Pb/^{204}Pb$ and $^{207}Pb/^{204}Pb$ vs. $^{206}Pb/^{204}Pb$ indicates that there have been no additions or major fractionation of U/Pb or Th/Pb in the crust since the amalgamation of the Tanzanian Craton in a convergent margin setting ca. 2.7 Ga.

8. Conclusions

The Pb isotopic composition of feldspars from lower crustal xenoliths from the Tanzanian Craton, in combination with previous studies on surface samples and mantle xenoliths indicate that the crust and lithospheric mantle comprising the Tanzanian Craton formed in the Archean in a convergent margin setting at approximately the same time, ca. ~2.7 Ga. Using a single-stage Pb evolution model, the crust of the Tanzanian Craton was extracted from a mantle with a $^{238}U/^{204}Pb$ of 8.1 ± 0.3 and $^{232}Th/^{238}U$ of 4.3 ± 0.1. Single anti-perthitic feldspars have isochrons that have an average age of 2.4 Ga, which indicates the time at which the lower crust cooled to a

temperature <600 °C. After 2.4 Ga, the temperature of the Tanzanian Craton lower crust, as represented by the xenoliths examined here, did not rise above 600 °C during either the Pan-African Orogeny or the present-day rifting. The identical common Pb isotopic compositions of the surface samples and lower crust indicate that there was no addition, subtraction, or fractionation of U, Pb, or Th in the crust of the Tanzanian Craton since its formation ca. 2.7 Ga.

Acknowledgements

We thank Phil Piccoli for help with image captures using the electron microprobe. We also thank Drs. Richard Ash and Igor Puchtel for lab assistance and Ricardo Arevalo, Jr. for thoughtful discussions. We thank Madalyn Blondes for many discussions and for providing the geological map of the area. We thank Andreas Möller, Mark Schmitz, Simon Johnson, and an anonymous reviewer for their insightful comments on this and an earlier version of this paper. This work was supported by the National Science Foundation (grant EAR0337255) and the National Geographic Society (grant 7836-05).

Appendix A. Supplementary data

Supplementary data to this article can be found online at doi:10.1016/j.epsl.2010.11.031.

References

Aulbach, S., Rudnick, R.L., McDonough, W.F., 2008. Li–Sr–Nd isotope signatures of the plume and cratonic lithospheric mantle beneath the margin of the rifted Tanzanian Craton (Labait). Contrib. Mineralog. Petrol. 155, 79–92.

Baker, J., Peate, D., Waight, T., Meyzen, C., 2004. Pb isotopic analysis of standards and samples using a Pb-207–Pb-204 double spike and thallium to correct for mass bias with a double-focusing MC-ICP-MS. Chem. Geol. 211 (3–4), 275–303.

Blondes, M.S., Rudnick, R.L., Bowring, S.A., Piccoli, P.M., Ramezani, J., 2009. Thermal history of the deepest parts of orogens through U–Pb thermochronology of Tanzanian deep crustal xenoliths. EOS Transactions, AGU, Fall Meeting Supplemental Abstract (V13E-2073).

Bolhar, R., Kamber, B.S., Collerson, K.D., 2007. U–Th–Pb fractionation in Archean lower continental crust: implications for terrestrial Pb isotope systematics. Earth Planet. Sci. Lett. 254 (1–2), 127–145.

Boyd, F.R., 1973. A pyroxene geotherm. Geochim. Cosmochim. Acta 37, 2533–2546.

Burton, K., Schiano, P., Birck, J., Allegre, C., Rehkamper, M., Halliday, A., Dawson, J., 2000. The distribution and behaviour of rhenium and osmium amongst mantle minerals and the age of the lithospheric mantle beneath Tanzania. Earth Planet. Sci. Lett. 183 (1–2), 93–106.

Carlson, R.W., Pearson, D.G., James, D.E., 2005. Physical, chemical, and chronological characteristics of the continental mantle. Rev. Geophys. 43, 2–24.

Chapman, D.S., Pollack, H.N., 1977. Regional geotherms and lithospheric thickness. Geology 5, 265–268.

Chauvel, C., Dupre, B., Arndt, N.T., 1993. Pb and Nd isotopic correlation in Belingwe komatiites and basalts. In: Bickle, M.J., Nisbet, E.G. (Eds.), The Geology of the Belingwe Greenstone Belt, Zimbabwe: A Study of the Evolution of Archean Continental Crust: Balkema, Rotterdam: Geological Society of Zimbabwe Special Publication, 2, pp. 167–174.

Chen, J., Wasserburg, G., 1983. The isotopic composition of silver and lead in 2 iron-meteorites—Cape-York and Grant. Geochim. Cosmochim. Acta 47 (10), 1725–1737.

Cherniak, D.J., 1995. Diffusion of lead in plagioclase and K-feldspar—an investigation using Rutherford backscattering and resonant nuclear-reaction analysis. Contrib. Mineralog. Petrol. 120 (3–4), 358–371.

Cherniak, D.J., Lanford, W.A., Reyerson, F.J., 1991. Lead diffusion in apatite and zircon using ion-implantation and Rutherford backscattering techniques. Geochim. Cosmochim. Acta 55 (6), 1663–1673.

Chesley, J.T., Rudnick, R.L., Lee, C.T., 1999. Re–Os systematics of mantle xenoliths from the East African Rift: age, structure, and history of the Tanzanian Craton. Geochim. Cosmochim. Acta 63 (7–8), 1203–1217.

Collins, A., Reddy, S., Buchan, C., Mruma, A., 2004. Temporal constraints on Palaeoproterozoic eclogite formation and exhumation (Usagaran Orogen, Tanzania). Earth Planet. Sci. Lett. 224 (1–2), 175–192.

Coomer, P.G., Robertson, D.K., 1974. A lead isotope study of Archean mineralized areas in Tanzania. J. Geol. Soc. 130, 449–460.

Cutten, H., Johnson, S.P., De Waele, B., 2006. Protolith ages and timing of metasomatism related to the formation of whiteschists at Mautia Hill, Tanzania: implications for the assembly of Gondwana. J. Geol. 114 (683–698).

Dawson, J. B. (1992). Neogene tectonics and volcanicity in the North Tanzania sector of the Gregory rift-valley—contrasts with the Kenya sector. Tectonophysics, 204(1–2):81–92. 15.

Dawson, J., James, D., Paslick, C., Halliday, A., 1997. Ultrabasic potassic low-volume magmatism and continental rifting in north-central Tanzania: association with enhanced heat flow. Geol. Geofiz. 38 (1), 67–77.

de Laeter, J.R., Bohlke, J.K., Bievre, P.D., Hidaka, H., Peiser, H.S., Rosman, K.J.R., Taylor, P.D.P., 2003. Atomic weights of the elements: review 2000. Pure Appl. Chem. 75 (6), 683–800.

Dodson, M.H., 1973. Closure temperature in cooling geochronological and petrological systems. Contrib. Mineralog. Petrol. 40, 259–274.

Dupré, B., Arndt, N.T., 1990. Pb isotopic compositions of Archean komatiites and sulfides. Chem. Geol. 85, 35–56.

Farmer, G.L., 2003. Continental basaltic rocks. In: Rudnick, R.L. (Ed.), Treatise on Geochemistry—Chapter 3, The Crust. Elsevier-Pergamon, Oxford, pp. 85–121.

Frei, R., Kamber, B.S., 1995. Single mineral Pb–Pb dating. Earth Planet. Sci. Lett. 129 (1–4), 261–268.

Frei, R., Villa, I.M., Nagler, T.F., Kramers, J.D., Przybylowicz, W.J., Prozesky, V.M., Hoffman, B.A., Kamber, B.S., 1997. Single mineral dating by the Pb–Pb step-leaching method: assessing the mechanisms. Geochim. Cosmochim. Acta 61 (2), 393–414.

Fritz, H., Tenczer, V., Hauzenberger, C., Wallbrecher, E., Muhongo, S., 2009. Hot granulite nappes—tectonic styles and thermal evolution of the Proterozoic granulite belts in East Africa. Tectonophysics 477 (3–4), 160–173 Sp. Iss. SI.

Holmes, A., 1946. An estimate of the age of the Earth. Nature 157, 680–684.

Housh, T., Bowring, S.A., 1991. Lead isotopic heterogeneities within alkali feldspars—implications for the determination of initial lead isotopic compositions. Geochim. Cosmochim. Acta 55 (8), 2309–2316.

Houtermans, F., 1946. Die Isotopenhaufigkeiten im naturlichen Blei und das Alter de Urans. Naturwissenschaften 33, 185–286.

Johnson, S.P., Cutten, H.N.C., Muhongo, S., Waele, B., 2003. Neoarchean magmatism and metamorphism of the western granulites in the central domain of the Mozambique belt, Tanzania: U–Pb shrimp geochronology and PT estimates. Tectonophysics 375 (1–4), 125–145.

Kamber, B.S., Collerson, K.D., Moorbath, S., Whitehouse, M.J., 2003. Inheritance of early Archean Pb-isotope variability from long-lived Hadean protocrust. Contrib. Mineralog. Petrol. 145, 25–46.

Kent, A.J.R., 2008a. *In situ* analysis of Pb isotope ratios using laser ablation MC-ICP-MS: controls on precision and accuracy and comparison between Faraday cup and ion counting systems. J. Anal. At. Spectrom. 23 (7), 968–975.

Kent, A.J.R., 2008b. Lead isotope homogeneity of NIST SRM 610 and 612 glass reference materials: constraints from laser ablation multicollector ICP-MS (LA–MC-ICP-MS) analysis. Geostand. Geoanal. Res. 32 (2), 129–147.

Lee, C.T., Rudnick, R.L., 1999. Compositionally stratified cratonic lithosphere: petrology and geochemistry of peridotite xenoliths from the Labait tuff cone, Tanzania. Proceedings of the Seventh International Kimberlite Conference, pp. 503–521.

Ludwig, K.R., 2003. User's Manual for Isoplot 3.00 a Geochronological Toolkit for Microsoft Excel, Berkeley Geochronology Center Special Publication No. 4.

Ludwig, K.R., Silver, L.T., 1977. Lead-isotope inhomogeneity in Precambrian igneous K-feldspars. Geochim. Cosmochim. Acta 41 (10), 1457–1471.

Maboko, M.A.H., 2000. Nd and Sr isotopic investigation of the Archean–Proterozoic boundary in north eastern Tanzania: constraints on the nature of Neoproterozoic tectonism in the Mozambique Belt. Precambrian Res. 102 (1–2), 87–98.

Mansur, A. (2008). Composition, age, and origin of the lower crust in northern Tanzania. Master's Thesis, University of Maryland College-Park. http://hdl.handle.net/1903/8993.

Manya, S., Kobayashi, K., Maboko, M.A.H., Nakamura, E., 2006. Ion microprobe zircon U–Pb dating of the late Archean metavolcanics and associated granites of the Musoma–Mara Greenstone Belt, Northeast Tanzania: implications for the geological evolution of the Tanzania Craton. J. Afr. Earth Sci. 45 (3), 355–366.

Michuat, C., Jaupart, C., Bell, D., 2007. Transient geotherms in Archean continental lithosphere: new constraints on thickness and heat production of the subcontinental lithospheric mantle. J. Geophys. Res. Solid Earth 112 (B4), B04408.

Möller, A., Appel, P., Mezger, K., Schenk, V., 1995. Evidence for a 2 Ga subduction zone-eclogites in the Usagaran belt of Tanzania. Geology 23 (12), 1067–1070.

Möller, A., Mezger, K., Schenk, V., 1998. Crustal age domains and the evolution of the continental crust in the Mozambique Belt of Tanzania: combined Sm–Nd, Rb–Sr, and Pb–Pb isotopic evidence. J. Petrol. 39 (4), 749–783.

Nyblade, A., Brazier, R., 2002. Precambrian lithospheric controls on the development of the East African rift system. Geology 30 (8), 755–758.

Nyblade, A.A., Pollack, H.N., 1993. A global analysis of heat-flow from Precambrian terrains—implications for the thermal structure of Archean and Proterozoic lithosphere. J. Geophys. Res. Solid Earth 98 (B7), 12207–12218.

Nyblade, A.A., Pollack, H.N., Jones, D.L., Podmore, F., Mushayanbedvu, M., 1990. Terrestrial heat-flow in East and Southern Africa. J. Geophys. Res. Solid Earth Planet. 95 (B11), 17371–17384.

Oversby, V., 1975. Lead isotope systematics of Archean acid intrusives in the Kalgoorlie–Norseman area, Western Australia. Geochim. Cosmochim. Acta 39, 1107–1125.

Oversby, V., 1978. Lead isotope systematics of Archean plutonic rocks. Earth Planet. Sci. Lett. 38 (1), 237–248.

Paslick, C., Halliday, A., James, D., Dawson, J.B., 1995. Enrichment of the continental lithosphere by OIB melts: isotopic evidence from the volcanic province of northern Tanzania. Earth Planet. Sci. Lett. 130, 109–126.

Paul, B., Woodhead, J.D., Hergt, J., 2005. Improved *in situ* isotope analysis of low-Pb materials using LA–MC-ICP-MS with parallel ion counter and faraday detection. J. Anal. At. Spectrom. 20 (12), 1350–1357.

Ritsema, J., Ni, S., Helmberger, D., Crotwell, H., 1998. Evidence for strong shear velocity reductions and velocity gradients in the lower mantle beneath Africa. Geophys. Res. Lett. 25 (23), 4245–4248.

Rudnick, R.L., 1992. Xenoliths—samples of the lower continental crust. In: Fountain, D.M., Arculus, R., Kay, R.W. (Eds.), Continental Lower Crust.

Rudnick, R.L., Goldstein, S.L., 1990. The Pb isotopic compositions of lower crustal xenoliths and the evolution of the lower crustal Pb. Earth Planet. Sci. Lett. 98, 192–207.

Rudnick, R.L., Nyblade, A.A., 1999. The composition and thickness of Archean continental roots: constraints from xenolith thermobarometry in Mantle Petrology: field observations and high-pressure experimentation: a tribute to Francis R. (Joe) Boyd. In: Fei, Y.-W., Bertka, C.M., Mysen, B.O. (Eds.), Geochemical Society Special Publications, 6, pp. 3–12.

Rudnick, R.L., McDonough, W.F., O'Connell, R.J., 1998. Thermal structure, thickness, and composition of continental lithosphere. Chem. Geol. 145, 395–411.

Rudnick, R.L., Ireland, T., Gehrels, G., Irving, A.J., Chesley, J.T., Hanchar, J.M., 1999. Dating mantle metasomatism: U–Pb geochronology of zircons in cratonic mantle xenoliths from Montana and Tanzania. In: Gurney, J.J., Gurney, J.L., Pascoe, M.D., Richardson, S.H. (Eds.), The Nixon Volume, Proceedings of the Seventh International Kimberlite Conference, pp. 728–735.

Schmitz, M.D., Bowring, S.A., 2003. Thermal structure, thickness, and composition of continental lithosphere. Contrib. Mineralog. Petrol. 144, 592–618.

Schulter, T., 1997. Geology of East Africa. Geology of East Africa. Borntraeger Verlagsbuchhandlung, Science Publishers, Stuttgart.

Smith, J., Brown, W., 1988. Crystal Structures, Physical, Chemical, and Microtextural Properties in Feldspar Minerals, 2nd edition. Springer Verlagsbuchhandlung, Heidelberg.

Stacey, J., Kramers, J., 1975. Approximation of terrestrial lead isotope evolution by a two-stage model. Earth Planet. Sci. Lett. 26, 207–221.

Weerarante, D., Forsyth, D., Fischer, K., Nyblade, A., 2003. Evidence for an upper mantle plume beneath the Tanzanian Craton from Rayleigh wave tomography. J. Geophys. Res. Solid Earth 108 (B9), 2427.

Zartman, R.E., Haines, E., 1988. The plumbotectonics model for Pb isotopic systematics among major terrestrial reservoirs—a case for bi-directional transport. Geochim. Cosmochim. Acta 52, 1327–1339.

Zartman, R.E., Richardson, S.H., 2005. Evidence from kimberlitic zircon for a decreasing mantle Th/U since the Archean. Chem. Geol. 220 (3–4), 263–283.

Zartman, R., Wasserburg, G., 1969. The isotopic composition of lead in potassium feldspars from some 1.0 By-old North American igneous rocks. Geochim. Cosmochim. Acta 33, 901–942.